**SANDIA REPORT**
SAND2007-3524
Unlimited Release
Printed August 2007

# Shock Response of Dry Sand

Justin L. Brown, Tracy J. Vogler, Lalit C. Chhabildas,
William D. Reinhart, and Tom F. Thornhill
Solid Dynamics and Energetic Materials Department

Prepared by
Sandia National Laboratories
Albuquerque, New Mexico 87185 and Livermore, California 94550

Sandia is a multiprogram laboratory operated by Sandia Corporation,
a Lockheed Martin Company, for the United States Department of Energy's
National Nuclear Security Administration under Contract DE-AC04-94AL85000.



Issued by Sandia National Laboratories, operated for the United States Department of Energy by Sandia Corporation.



Available to DOE and DOE contractors from
U.S. Department of Energy
Office of Scientific and Technical Information
P.O. Box 62
Oak Ridge, TN 37831

Telephone: (865) 576-8401
Facsimile: (865) 576-5728
E-Mail: reports@adonis.osti.gov
Online ordering: http://www.osti.gov/bridge

Available to the public from
U.S. Department of Commerce
National Technical Information Service
5285 Port Royal Rd.
Springfield, VA 22161

Telephone: (800) 553-6847
Facsimile: (703) 605-6900
E-Mail: orders@ntis.fedworld.gov
Online order: http://www.ntis.gov/help/ordermethods.asp?loc=7-4-0#online

SAND2007-3524
Unlimited Release
Printed August 2007

# Shock Response of Dry Sand

Justin L. Brown, Tracy J. Vogler, Lalit C. Chhabildas,
William D. Reinhart, and Tom F. Thornhill

Solid Dynamics and Energetic Materials
Sandia National Laboratories
P.O. Box 5800
Albuquerque, New Mexico 87185-MS1181

**Abstract**

The dynamic compaction of sand was investigated experimentally and computationally to stresses of 1.8 GPa. Experiments have been performed in the powder's partial compaction regime at impact velocities of approximately 0.25, 0.5, and 0.75 km/s. The experiments utilized multiple velocity interferometry probes on the rear surface of a stepped target for an accurate measurement of shock velocity, and an impedance matching technique was used to deduce the shock Hugoniot state. Wave profiles were further examined for estimates of reshock states. Experimental results were used to fit parameters to the P-Lambda model for porous materials. For simple 1-D simulations, the P-Lambda model seems to capture some of the physics behind the compaction process very well, typically predicting the Hugoniot state to within 3%.

## ACKNOWLEDGMENTS

The authors would like to thank Heidi Anderson for the assembly of the target fixtures, and the STAR team for the execution of the experiments.

# CONTENTS



# FIGURES



# TABLES

# 1. INTRODUCTION

The dynamic behavior of sand and other granular ceramics is of fundamental importance to a variety of engineering applications. Examples include seismic coupling, planetary science applications, penetration, and the performance of ceramic armors.

Although the behavior of sand has been studied extensively, its dynamic behavior remains poorly understood. High-quality experimental data are needed for computational simulations of dynamic events involving sand and also to improve our understanding of granular physics.

Several models have been proposed to describe the dynamic compaction of porous materials. Among the most widely used is the P-$\alpha$ model [1]. While the model is relatively simple and largely empirical, it captures many of the important features of dynamic compaction, while requiring only a few material parameters which can be easily found or estimated. More recently, the P-$\alpha$ model has been generalized to accommodate multi-phase mixtures in the form of the P-$\lambda$ model [2, 3]. Both models have been implemented in the CTH hydrocode, but calibration of the models for different materials has generally not been performed.

In this report, we describe a series of experiments to measure the shock behavior of sand in the partially compacted region to stresses of 1.8 GPa. These results are compared to shock data for sand from the literature. The results of these experiments are used to obtain model parameters for the P-$\alpha$ and P-$\lambda$ models for dry sand.

# 2. EXPERIMENTAL TECHNIQUE

## 2.1. Material

A variety of silica sand was used in this investigation. The measured average density of the samples was 1.57 g/cm$^3$ or approximately 59% of full density. The sand's morphology is illustrated in Figure 1.

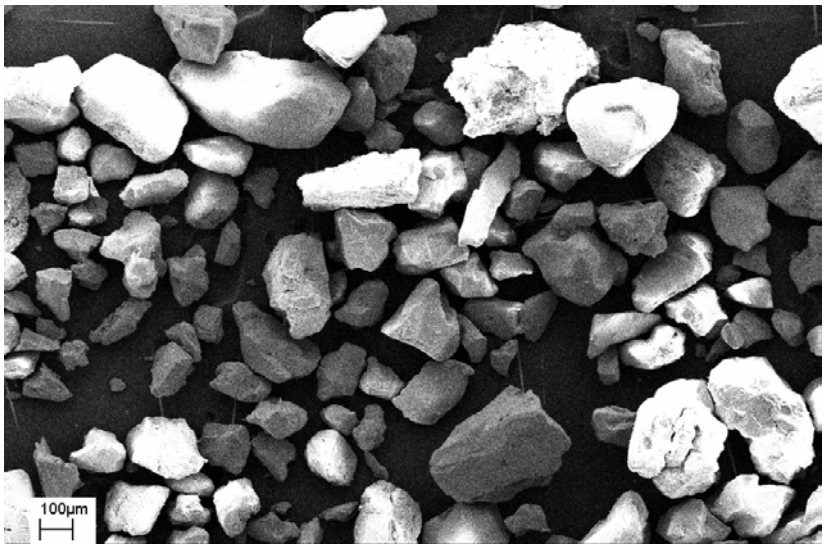


**Figure 1. SEM image of untested sand powder.**

## 2.2. Configuration

A special fixture, shown in Figure 2, was developed in order to provide an accurate measurement of shock velocity. The current fixture is a simplified version of one used previously for tungsten carbide powder experiments [4]. The fixture was designed to be used on a 102 mm bore light gas gun, which operates by the release of compressed gas and can achieve projectile velocities as high as 900 m/s. The fixture was machined from a block of PMMA (polymethyl methacrylate) using computer-controlled tooling. A polymer was used so that wave speeds in the fixture would be as low as possible to reduce effects due to edge release. Secondary considerations leading to the choice of PMMA include machinability and its compatibility with glue used to attach other pieces to the fixture.

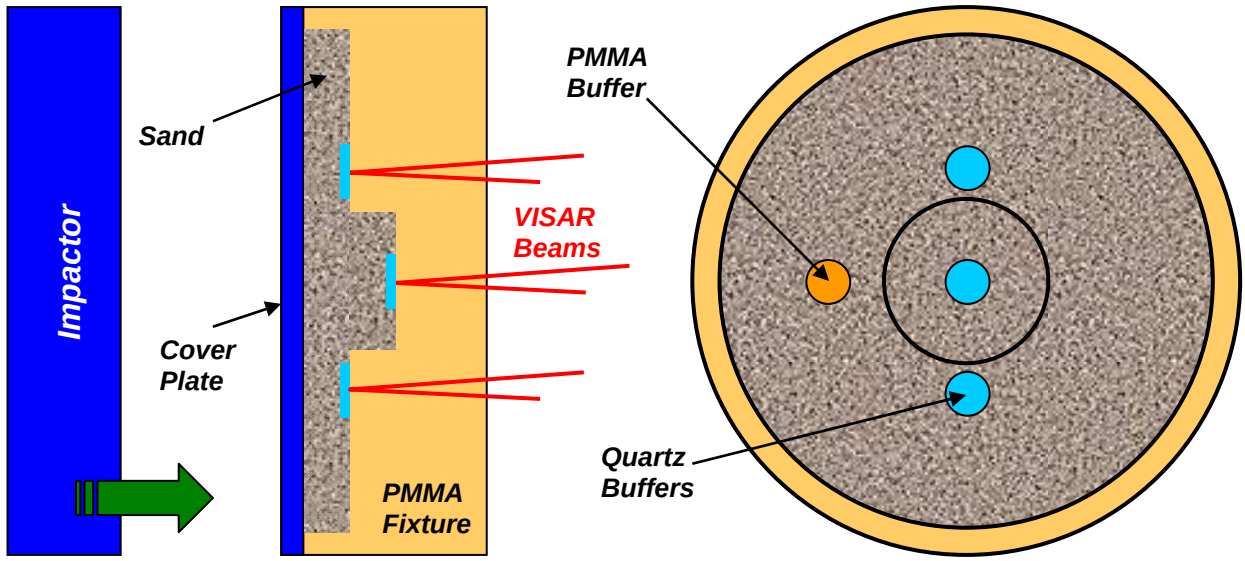


**Figure 2. Cross-section of the test fixture illustrating the use of two thicknesses to measure shock velocity (not to scale).**

A photograph of a completed fixture is shown in Figure 3. Its outer diameter was 89 mm, while the diameters of the first and second steps were 76 mm and 30 mm, respectively. The fixture thickness was 18 mm, and the steps, measured from the impact face of the fixture, were 3 to 3.5 mm and 5.5 to 6 mm thick. Z-cut quartz or PMMA buffers, 8 mm in diameter and 0.5 or 1.0 mm thick, were glued in place at the appropriate levels, as shown in Figure 2. A fiber optic probe was centered at each buffer, and a velocity interferometer system for any reflector (VISAR) [5] was used to monitor the vapor deposited aluminum spots on the PMMA at the interface between the quartz and PMMA. Quartz and PMMA buffers were used in an attempt to measure the reshock and release states of the sand, respectively. The open part of the fixture was filled with sand and a 1.5 mm thick fused silica or 3 mm thick 6061-T6 aluminum cover plate was glued on as shown in Figure 2. A vent hole in the top of the cavity facilitated evacuation of the powder, while a filter made of porous alumina placed in the vent prevented powder from being sucked out of the fixture. Evacuation leads to settling of the powder, so the fixture was pre-evacuated and additional powder was added through a small screw hole. The density of the sample was calculated using the measured volume of the fixture cavity and mass of the powder. Based on the variation in sample densities, random errors in the density are estimated to be 2-3%.

After fixture assembly was complete, it was glued into an aluminum target plate fit with velocity and tilt pins. Three shorting pins of varying height above the target were used to estimate the projectile velocity to within 0.5%. Similarly, four shorting pins just above the surface of the target were used to estimate projectile tilt. Projectile tilt was less than 2 mrad for all experiments. The target was then aligned and mounted onto the end of a single stage light gas gun. A 25 mm thick fused silica or 6061-T6 aluminum projectile was utilized for a symmetric impact with the fixture cover plate.

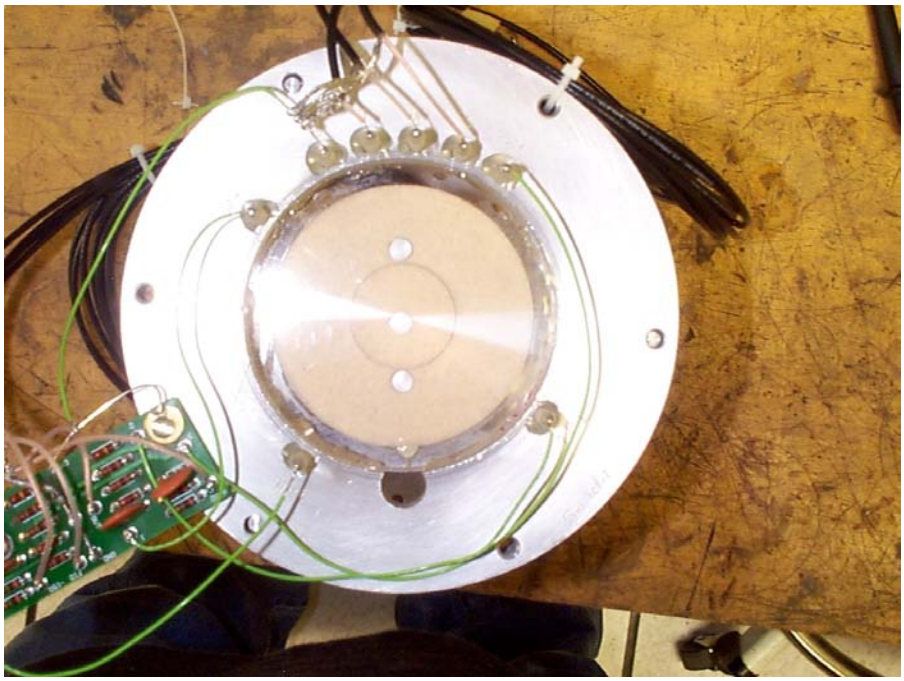

**Figure 3. Photograph of assembled fixture and target plate. The outer diameter of the target plate is 158.75 mm.**

# 3. EXPERIMENTAL RESULTS

A total of six shock experiments were performed on dry sand. A summary of the experimental configurations is given in Table 1. Velocity histories from these shots are used to determine the shocked state of the sand.

**Table 1. Summary of Experimental Configurations**

| Shot # | Projectile Velocity (km/s) | $\rho_{00}$ (g/cc) | Projectile Material | Cover Plate Material | Cover Plate Thickness (mm) |
|---|---|---|---|---|---|
| Sand-1[1] | 0.263 | 1.54 | Fused Silica | Fused Silica | 1.58 |
| Sand-2[1] | 0.500 | 1.56 | Fused Silica | Fused Silica | 1.65 |
| Sand-3[1] | 0.699 | 1.53 | Al | Al | 3.07 |
| Sand-4 | 0.257 | 1.59 | Al | Al | 3.08 |
| Sand-5 | 0.503 | 1.56 | Al | Al | 3.07 |
| Sand-6 | 0.752 | 1.61 | Al | Al | 3.07 |

1 Shot did not contain PMMA buffer

## 3.1. Velocity History Results

Velocity histories were obtained for the buffer/PMMA interfaces shown in Figure 2. These results are illustrated by a detailed description of a typical experiment. First, the velocity pin data is examined and relative times for which the pins shorted can be compared with the relative heights of the pins to obtain an average projectile velocity. Next, tilt pins are used to calculate a least squares fit of arrival times in space, resulting in a correction time for each signal. The VISAR signals are correlated using a common digital fiducial and after correcting for tilt and time of impact, the profiles in Figure 4a are obtained. The PMMA signal arrives later because wave speeds are slower for PMMA. Figure 4b shows an overlay of all the profiles. In all experiments, the responses are terminated when edge release waves are expected to arrive.

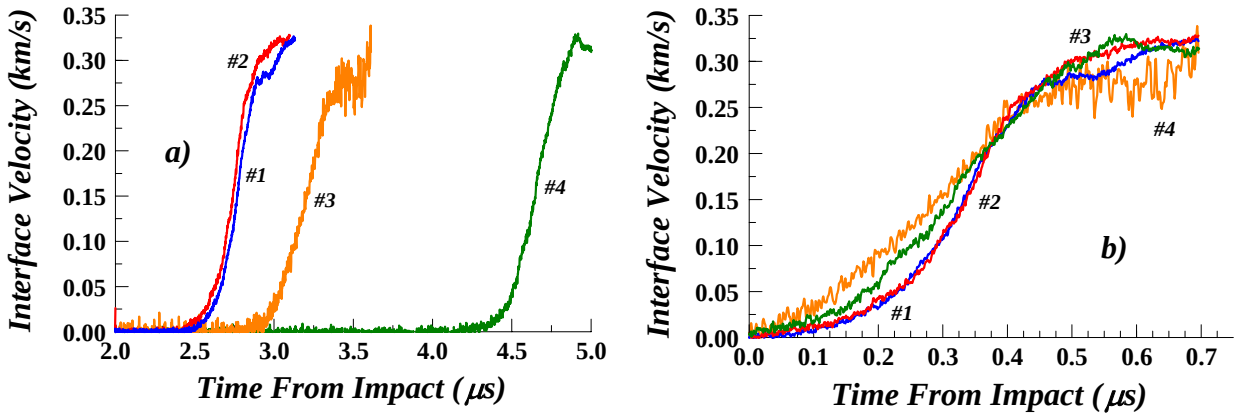


**Figure 4. Velocity histories from a typical experiment a) correlated to time of impact and b) shifted in time to overlay. Probes #1, #2, and #4 utilize a quartz buffer.**

## 3.2. Determination of the shock Hugoniot state

The Hugoniot state for sand was determined using the measured VISAR profiles and impedance matching with the known properties of the impactor and cover plate. The midpoint of rise in the VISAR profiles were used to determine the shock velocity in the sand by measuring the arrival time of each profile measured through a quartz buffer (Probes #1, #2, and #4 in Figure 4). Ideally, the profiles measured at the same sample thickness should be identical. Experimental errors, however, produce differences in arrival times on the order of 100 ns. An average of these times gives the shock arrival time at the first fixture thickness. Comparing this time to the signal arrival of the second fixture thickness gives the shock transit time through the sand. The measured displacement through which the shock travels over this time yields an accurate measurement of the shock velocity in the sand.

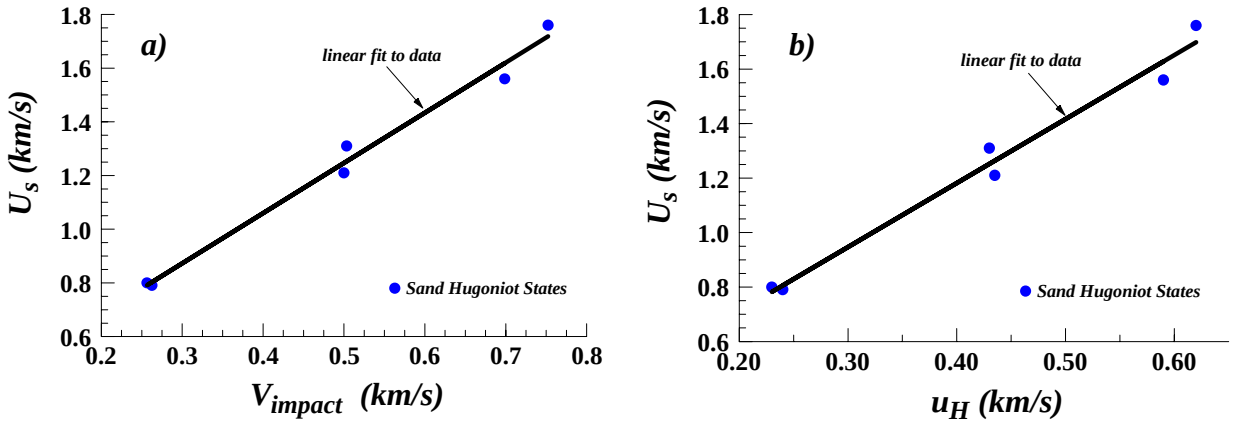


**Figure 5. Measured shock velocity as a function of a) impact velocity and b) sand Hugoniot particle velocity along with linear fits of the data.**

A linear correlation between the calculated shock velocity, $U_s$, and impact velocity, $V_{impact}$, represents the data well over the range of these experiments, as shown in Figure 5a.

The best fit is given by

$$U_s = 1.8686 + 0.3125 V_{impact}. \quad \textbf{(1)}$$

The shocked state after impact in the projectile and cover plate is determined from the symmetry condition for particle velocity, $u_p = 0.5 V_{impact}$, and the known Hugoniot of the material (fused silica or aluminum). When the shock wave passing through the cover plate reaches the sand, it releases to the Hugoniot for sand. The Hugoniot is constrained to lie on this release path and along a Rayleigh line from the origin with slope given by

$$\frac{\Delta\sigma}{\Delta u_p} = \rho_{00} U_s, \quad \textbf{(2)}$$

where $\sigma$ is the stress in the direction of shock propagation in the sand (positive in compression). This technique is illustrated graphically in Figure 6. The Rayleigh lines are based upon the initial densities given in Table 1 and the calculated shock velocity.

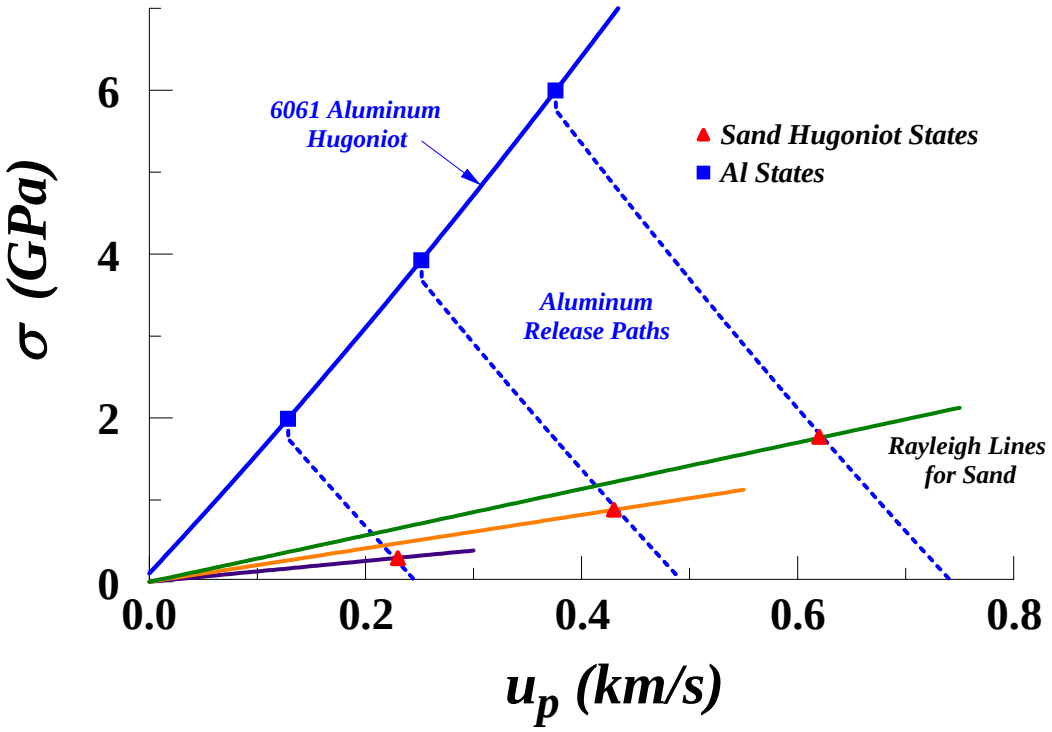


**Figure 6. $\sigma$-$u_p$ diagram illustrating impedance matching of an aluminum projectile impacting an aluminum cover plate and sand sample to determine the Hugoniot state of the sand. The intersection of the Rayleigh line with the corresponding aluminum release path determines the Hugoniot particle velocity and stress state of the sand.**

For aluminum, the Hugoniot data obtained by Wallace [6] from unsteady wave propagation in 6061-T6 aluminum [7] are used. For stresses somewhat above the Hugoniot elastic limit (HEL) but below about 10 GPa, the data can be expressed extremely well using the quadratic form

$$\sigma = 0.10387 + 14.203u_p + 3.9024u_p^2. \quad \textbf{(3)}$$

The unloading path of aluminum is constructed in the following manner. First, the Hugoniot described by Equation (3) is displaced downward by 4/3Y, where Y is the yield stress of aluminum. For Y, the value obtained during release experiments [8] on this material of 0.18 GPa is used. This value for Y represents a lower bound since the value at the HEL was found to be 0.26 GPa. Initial unloading is assumed to be elastic at a slope given by Equation (2) with the wavespeed for an elastic precursor in aluminum of 6.5 km/s [6] used for $U_s$. Elastic unloading is assumed to terminate when this line intersects the displaced curve from Equation (3), effectively assuming elastic-perfectly plastic unloading. This is known not to be entirely correct [8] but is sufficiently accurate for the current purposes.

For the two fused silica experiments, the impedance matching is simplified. The Hugoniot data obtained by Barker [9] is estimated to be nonlinearly elastic to at least 6.5 GPa and may be expressed by the 4$^{th}$ order polynomial

$$\sigma = 13.17u_p + 7.361u_p^2 + 9.947u_p^3 + 4.163u_p^3. \quad \textbf{(4)}$$

In these experiments the stresses in the fused silica do not exceed 3 GPa, so the unloading may be assumed to be elastic, and is a direct reflection of the Hugoniot expressed in Equation (4) through the symmetric impact state.

For all experiments in the current investigation, the intersection of the release path and the Rayleigh line for the sand occurs in the region of elastic unloading of the cover plate. Errors associated with impedance matching are estimated to be less than 2% in $\sigma$ and $u_p$ and are due primarily to the uncertainty in the Hugoniots over this regime. Once the particle velocity is determined, the Hugoniot density is calculated as

$$\rho_H = \rho_{00} \frac{U_s}{U_s - u_H}, \quad \textbf{(5)}$$

where the subscript H denotes the Hugoniot state.

## 3.3. Shock Hugoniot state

Hugoniot data for all experiments is given in Table 2. The linear correlation between $U_s$ and $u_H$ (Figure 5b) was found to be

$$U_s = 0.243 + 2.348u_H. \quad \textbf{(6)}$$

**Table 2. Hugoniot results for sand experiments**

| Shot # | $U_s$ (km/s) | $u_H$ (km/s) | $\sigma_H$ (GPa) | $\rho_H$ (g/cm$^3$) |
|---|---|---|---|---|
| Sand-1 | 0.79 | 0.24 | 0.29 | 2.22 |
| Sand-2 | 1.21 | 0.44 | 0.82 | 2.46 |
| Sand-3 | 1.56 | 0.59 | 1.42 | 2.49 |
| Sand-4 | 0.80 | 0.23 | 0.29 | 2.25 |
| Sand-5 | 1.31 | 0.43 | 0.88 | 2.35 |
| Sand-6 | 1.76 | 0.62 | 1.77 | 2.51 |

Hugoniot states with the fit given by Equation (6) are plotted in the σ-ρ plane in Figure 7, along with a fit of the P-λ model [2, 10] using the experimental data in Table 2. The calculated constants for the model are $p_c$ = 115 MPa, and n = 0.3, relating to the ensemble strength on a cellular level, and homogeneity of the compaction transition, respectively. As shown, the P-λ model captures the response of sand well, typically within 3%, over the range of these experiments. A more detailed discussion of the P-λ model and these parameters is given in section 3.4.

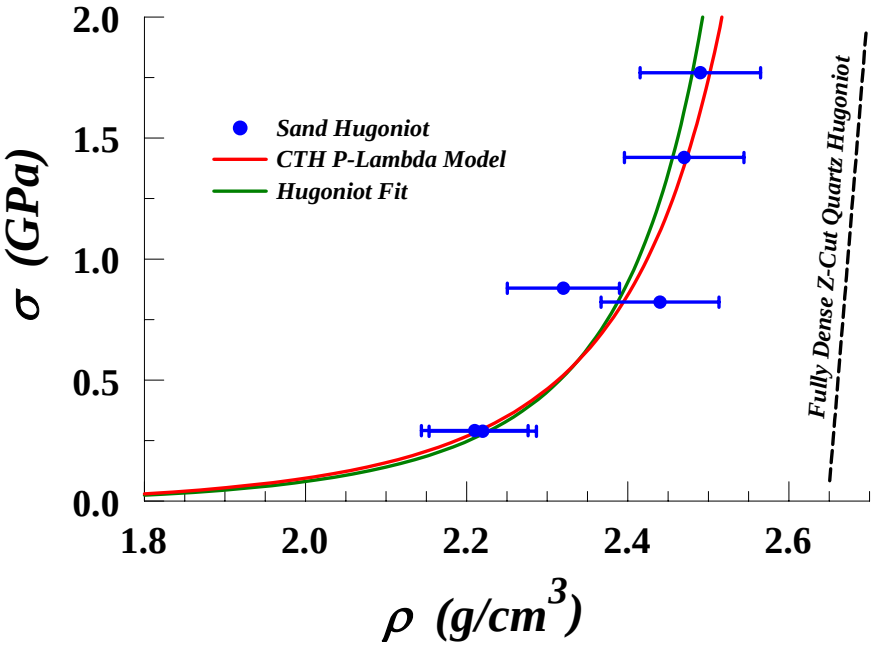


**Figure 7. Shock response of sand along with the Hugoniot of fully dense Z-Cut Quartz. A fit of the Hugoniot data along with the P-λ fit are also given.**

For reference, the results obtained in these experiments were compared with five sets of data from previous shock experiments on dry sand. Lagunov and Stepanov provide shock data on sand with an initial density of 1.66 g/cm$^3$ [11]. Tsembelis et al. performed plate impact experiments on sand with a bulk density of 1.45 g/cm$^3$ and grain sizes on the order of 0.15 mm [12]. The LLNL database contains shock data on sand with an initial density of 1.6 g/cm$^3$ and grain sizes less than 1mm [13]. Finally, Dianov et al. provide shock data on four different morphologies of sand [14]. Two of these data sets are applicable to the current study and are utilized here, with initial densities of 1.49 and 1.29 g/cm$^3$, and grain sizes of 0.07-0.14 and 0.07 mm, respectively. As shown in Figure 8, the particle morphology and initial density seem to play large roles in the dynamic response of the sand. For very small grain sizes, it appears the response is much stiffer, which is not unexpected as smaller grains result in higher particle strengths. Data sets also agree well with each other for similar grain sizes in terms of the shape of the response. It should also be noted that differences in experimental techniques could also play a large role in the discrepancies between data sets.

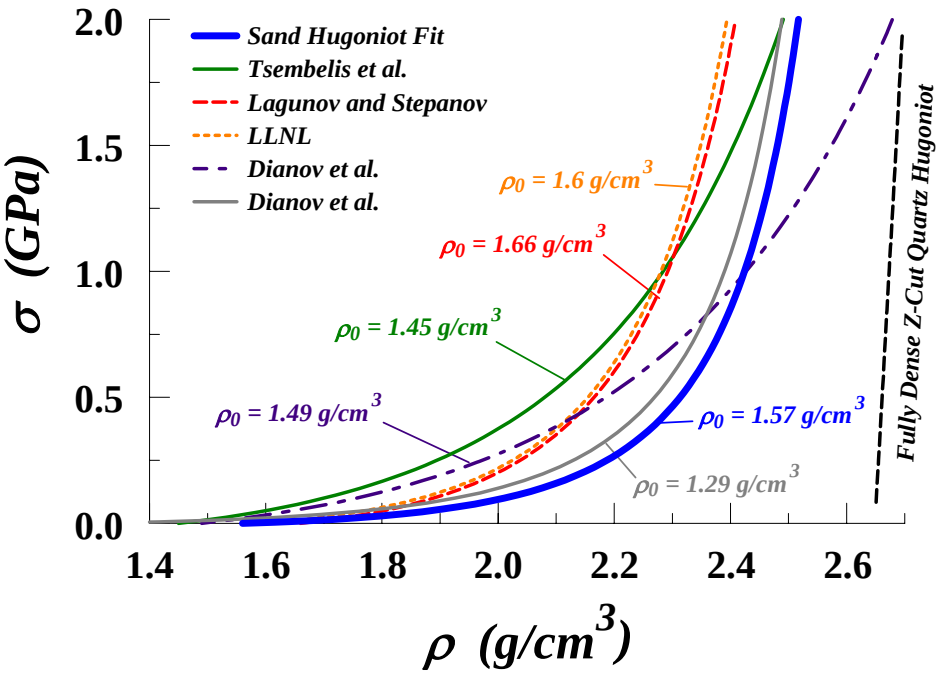


**Figure 8. Shock response of several varieties of sand along with the Hugoniot of fully dense Z-Cut Quartz.**

## 3.4. Determination of CTH P-λ model Parameters

Upper and lower bounds, known as the Voigt and Reuss bounds, for the compaction of porous materials may be calculated using iso-strain and iso-pressure assumptions, respectively [2]. These bounds are only a function of the volume fractions and bulk moduli of the mixture components, and can easily be computed using quartz and vacuum as the constituents. The extent of the compaction can be defined in terms of the specific volume as a function of pressure,

$$\nu_m(p) = \lambda \nu_R(p) + (1-\lambda)\nu_V(p), \tag{7}$$

where λ is a functional expression for the compaction extent, and $\nu_R$ and $\nu_V$ are the Reuss and Voigt bounds, respectively. A form of λ found to be applicable to a wide range of transformation processes in heterogeneous media [2] is proposed as,

$$\lambda(p) = 1 - e^{-\left(p/p_c\right)^n}, \tag{8}$$

where $p_c$ and n are parameters relating to the ensemble strength on a cellular level, and homogeneity of the compaction transition, respectively [10]. An illustration of the development of the compaction curve is given in Figure 9a.

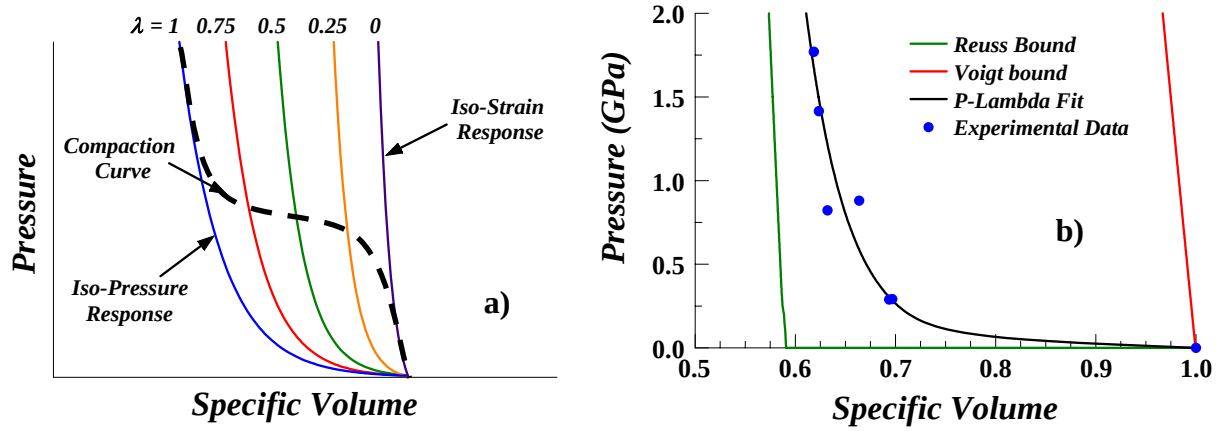


**Figure 9. Development of P-λ mixture curves in a) theory and b) for the experimental data.**

The Hugoniot data in Table 2 can be used to obtain the P-λ model parameters, $p_c$ and n. Each Hugoniot density (specific volume) and corresponding pressure may be used to calculate λ with Equation (7). Given the data points (p, λ), and the form of λ (Equation (8)), a least squares fit of the parameters can be performed.

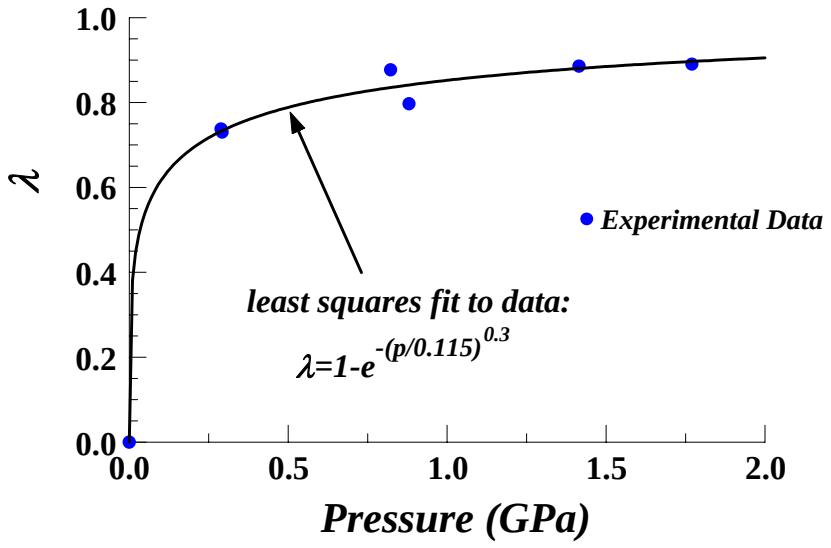


**Figure 10. P-λ CTH model fit to the experimental data.**

## 3.5. Determination of CTH P-α model Parameters

The p-alpha model, originally proposed by Hermann [1], provides a simple model for the compaction of porous materials through the utilization of a distention function, α. This function describes the ratio between the density of the porous material at pressure and the initial density of the solid, $\alpha(p)=\rho(p)/\rho_m$. While the distention function can be made to take a variety of forms, the most recent model implemented in the CTH hydrocode [15] is given by

$$\alpha(p) = 1 + (\alpha_0 - 1)\left(\frac{p_s - p}{p_s - p_e}\right)^n, \tag{9}$$

where $\alpha_0=\rho_{00}/\rho_m$, $p_e$ is the elastic pressure at the onset of compaction, ps is the pressure at which full compaction is achieved, and n is an arbitrary scaling parameter. A least squares fit of the parameters given by the model in Equation (9), yields $p_s$ =1.13 GPa, $p_e$ =0.9 Mpa, and n=1.4. While these parameters appear, at first glance, to be reasonable, a plot of the fit function, shown in Figure 11, shows that the model does not represent the data well. In particular, the obtained compaction pressure is much lower than the data suggests.

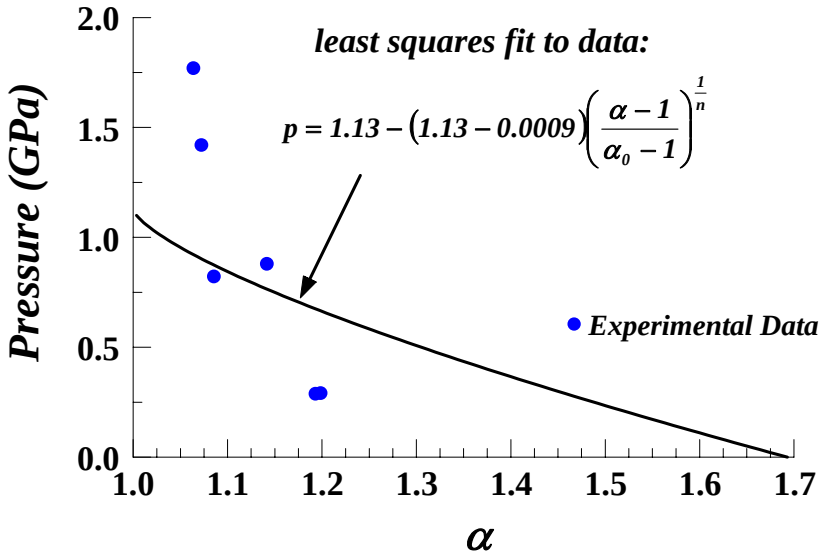


**Figure 11. P-α CTH model fit to the experimental data.**

An alternative form of the distention equation, suggested by Grady [16],

$$p(\alpha) = p_s \alpha^{-\eta}, \tag{10}$$

yields a best fit with the data with $p_s$=3.63 GPa and η=13.6. As shown in Figure 12a, this power-law model suggests a much more reasonable pressure of completion, and fits the data well. In an attempt to more accurately represent the data in CTH (Equation (9)), $p_s$ was taken from the power-law model, and $p_e$ was arbitrarily set to 0.01 GPa. The compaction curves are insensitive to the elastic pressure parameter, and have little effect on the results. The resulting CTH

compaction curves for varying values of n, given in Figure 12b, reinforce earlier sentiments that the CTH p-alpha model cannot accurately model the behavior of sand in these experiments.

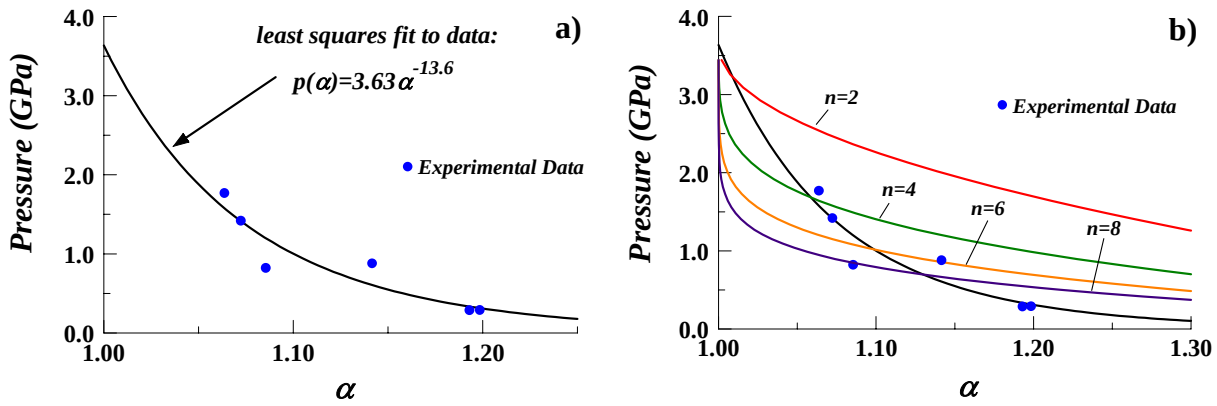


**Figure 12. P-α modified model fits to the experimental data.**

## 3.6. Off-Hugoniot State

Following impact, a shock wave traverses the cover plate and enters the sand sample, shocking it to its Hugoniot state, as discussed in section 3.2. Once the shock wave reaches the buffer, interactions at this interface causes the compressed sand to jump to a new stress state. These experiments attempted to capture both the reshock and release behavior of the compressed sand by using high and low impedance buffers. Z-cut quartz was expected to reshock the compressed sand, while PMMA was thought to release it.

The peak VISAR velocities determine the state of the shocked PMMA fixture. Impedance matching between the buffer and the fixture, in the case of the quartz buffer, gives the shocked state of the buffer. For the PMMA buffers, this is a trivial process. Since the particle velocity and longitudinal stress are continuous across the sand/buffer interface, these are known for the sand sample. An "inferred" off-Hugoniot velocity for the Lagrangian (undeformed) reference frame may then be calculated as

$$U_{sR} = \frac{\sigma_R - \sigma_H}{\rho_{00}(u_H - u_R)}, \tag{11}$$

where the subscript "H" denotes the Hugoniot state and the subscript "R" denotes the off-Hugoniot state (either reshock or release). Similarly, the density in the off-Hugoniot state can be calculated as

$$\rho_R = \rho_{00}\left(\frac{\rho_{00}}{\rho_H} - \frac{u_H - u_R}{U_{sR}}\right)^{-1}. \tag{12}$$

It should be noted that at lower impact velocities the arrival time of the peak VISAR velocity is very close to the expected arrival of the buffer edge release waves, which could result in a larger uncertainties in the measurements of the off-Hugoniot state.

**Table 3. Off-Hugoniot results for sand experiments**

| Shot # | Buffer Material | $u_R$ (km/s) | $\sigma_R$ (GPa) | $\rho_R$ (g/cm$^3$) |
|---|---|---|---|---|
| Sand-1 | Quartz | 0.125 | 2.15 | 2.25 |
| Sand-2 | Quartz | 0.2 | 3.4 | 2.57 |
| Sand-3 | Quartz | 0.26 | 4.6 | 2.7 |
| Sand-4 | Quartz | 0.09 | 1.45 | 2.32 |
| | PMMA | 0.165 | 0.6 | 2.3 |
| Sand-5 | Quartz | 0.2 | 3.6 | 2.43 |
| Sand-6 | Quartz | 0.32 | 5.94 | 2.63 |
| | PMMA | 0.61 | 2.45 | 2.49 |

The calculated off-Hugoniot states are given in Table 3, and a comparison with Table 2 will quickly show that all of the measured off-Hugoniot stresses are greater than the Hugoniot stress state, meaning the compressed sand was reshocked regardless of the buffer material. This can also be seen in Figure 4, where all of the measured waveforms exhibit a reshock response. This behavior may be attributed to the low density of sand. Previous work [4] focused on experiments with similar shock velocities, but higher densities, producing much steeper Rayleigh lines. All of the experiments in this work, however, result in Rayleigh lines lying below both the PMMA and the Z-cut quartz Hugoniots, making a reshock the only observed off-Hugoniot state for this configuration. A plot of the calculated reshock states is given in Figure 13. In most cases, the measured reshock states lie above the Hugoniot, as was the case for WC powder [4]. This suggests that the material is able to behave in a stiffer manner after being shocked.

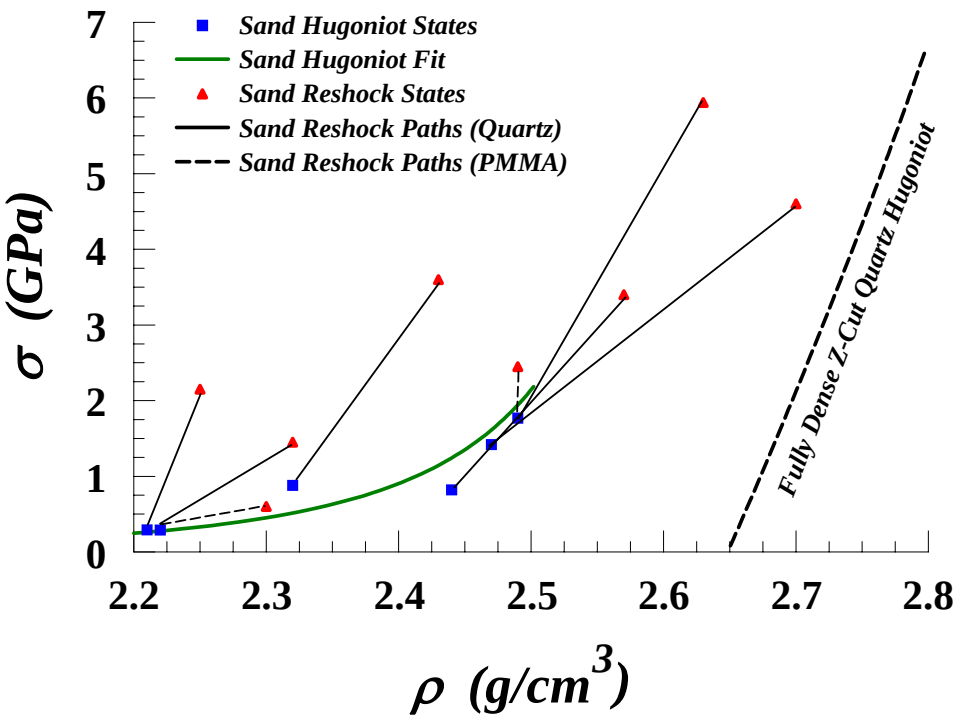


**Figure 13. Hugoniot and Reshock states attained by the sand.**

## 3.7. Strain Rate

In previous experiments [4], an interesting scaling relationship between stress and strain rate has been observed for steady waves in granular materials. Here, we examine the relationship between these quantities in the current experiments. The rise times of the waves are determined in the following manner. A line is constructed through the finite rise portion of waveform with a slope equal to the particle velocity history above the Hugoniot elastic limit (HEL) (see Figure 4). The times at which this line intersects horizontal lines representing the HEL and initial average peak value of the interface velocity are found. The difference between these times is taken to be the rise time of the wave. Strains are calculated through the correlation of initial and Hugoniot densities as shown in Equation (13), where ε is engineering strain (positive in compression).

$$\varepsilon = 1 - \frac{\rho_{00}}{\rho_H} \tag{13}$$

For several fully dense solids, an empirical relationship has been found between strain rate and stress, of the form

$$\dot{\varepsilon} \propto \sigma^n \tag{14}$$

where n is found to be approximately 4 [17]. If a similar relationship is assumed to hold for sand, a value of approximately 1 is found for the exponent, *n*. Similar analysis on ceramic powders produced values for *n* of 1.0 and 1.2 for $TiO_2$ [18] and WC [4], respectively.

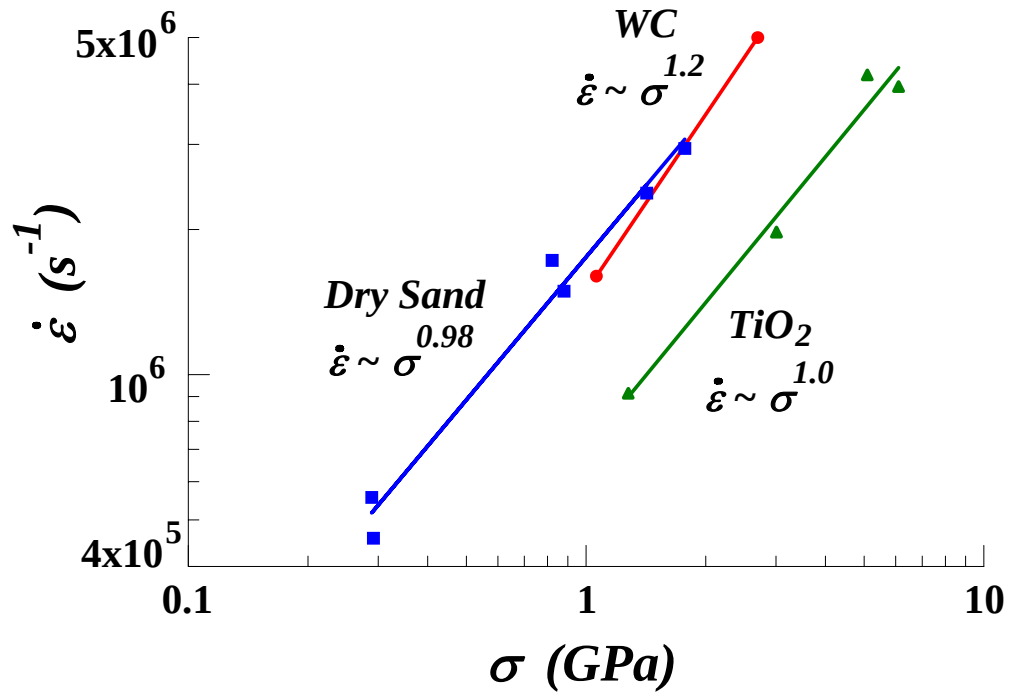


**Figure 14. Empirical relationship between strain rate and stress for several granular materials.**

# 4. DISCUSSION AND CONCLUSIONS

The dynamic compaction of 59% dense dry sand has been measured to 1.8 GPa. The experiments were conducted for several states of partial compaction using a novel experimental configuration in which the velocity of the compaction waves and the known response of the impactor and cover plate provide high quality Hugoniot data and time resolved measurements of material behavior. Experimental uncertainties in this configuration are estimated to be 3-3.6% in $\sigma_h$ and 2.5-2.7 in $\rho_h$. In addition to the shocked state, a reshock state was also determined from the measured VISAR velocity. While several new sources of error fall into the reshock calculation, the reshock states are consistently somewhat stiffer than the initial dynamic compaction response, suggesting some sort of elastic behavior upon reloading. The time resolved material response was also examined to obtain initial compaction wave rise times and strain rates. The empirical relationship between strain rate and stress ($\dot{\varepsilon} \sim \sigma^1$) was found to be much different from that of fully dense materials ($\dot{\varepsilon} \sim \sigma^4$), but consistent with other ceramic powders. The data obtained in these experiments were also compared to other results from the literature. While the qualitative response of other data sets is similar to the current data, differences in initial densities, grain sizes, and experimental techniques may have prevented a better correlation.

The current data set was also used to obtain parameters for computational modeling efforts in CTH using the P-$\alpha$ and P-$\lambda$ models. The P-$\lambda$ model parameters found to best fit the data is an ensemble cellular strength, $p_c$, of 115 MPa and a homogeneity of compaction, n, of 0.3. These parameters fit the experimental data extremely well, typically to within 3%. This simple model however, does not have an elastic reloading behavior built in, and reloading is constrained along the calculated Hugoniot. The current form of the P-$\alpha$ model in CTH, on the other hand, was unable to accurately represent the shock response of the sand. Instead, an alternate distention equation in the form of a power-law was found to fit the data very well. Implementation of this form of the equation should be considered for a more robust form of the P-$\alpha$ model.

## References


1. W. Herrmann, "Constitutive Equation for the Dynamic Compaction of Ductile Porous Materials," *Journal of Applied Physics,* vol. 10, pp. 2490-2499, 1969.
2. D. E. Grady, N. A. Winfree, G. I. Kerley, L. T. Wilson, and L. D. Kuhns, "Computational modeling and wave propagation in media with inelastic deforming microstructure," *Journal De Physique IV,* vol. 10, pp. 15-20, 2000.
3. D. E. Grady, "P-λ model for material mixtures: application to compaction of porous zirconium dioxide," Applied Research Associates report for contract 22278 and project 0775, 2001.
4. T. J. Vogler, M. Y. Lee, and D. E. Grady, "Static and dynamic compaction of ceramic powders," *International Journal of Solids and Structures,* vol. 44, pp. 636-658, 2007.
5. L. M. Barker and R. E. Hollenbach, "Laser interferometer for measuring high velocities of any reflecting surface," *Journal of Applied Physics,* vol. V43, pp. 4669-4675, 1972.
6. D. C. Wallace, "Equation of state from weak shocks in solids," *Physical Review B,* vol. 22, pp. 1495-1502, 1980.
7. J. N. Johnson and L. M. Barker, "Dislocation dynamics and steady plastic wave profiles in 6061-T6 aluminum," *Journal of Applied Physics,* vol. 40, pp. 4321-4334, 1969.
8. J. R. Asay and L. C. Chhabildas, "Determination of the shear strength of shock compressed 6061-T6 aluminum," in *Shock Waves and High-Strain-Rate Phenomena in Metals*, Plenum, New York, 1981, pp. 417-431.
9. L. M. Barker and R. E. Hollenbach, "Shock-wave studies of PMMA, fused silica, and sapphire," *Journal of Applied Physics,* vol. 41, pp. 4208-4226, 1970.
10. D. E. Grady and N. A. Winfree, "A computational model for polyurethane foam," in *Fundamental Issues and Applications of Shock-Wave and High-Strain-Rate Phenomena*, K. P. Staudhammer, L. E. Murr, and M. A. Meyers, Eds., 2001, pp. 485-491.
11. V. A. Lagunov and V. A. Stepanov, "Measuring measurements of the dynamic compressibility of sand," *Zhurnal Prikladnoi Mekhaniki i Tehknicheskoi Fiziki,* vol. 4, pp. 88-96, 1963.
12. K. Tsembelis, W. G. Proud, B. M. Vaughan, and J. E. Field, "The behavior of sand under shock wave loading: experiments and simulations," 14-15 November 2002 (unpublished).
13. M. van Thiel (Ed.), "Compendum of shock wave data," *Lawrence Livermore Laboratory Report UCRL-50108,* 1977.
14. M. Dianov, N. Zlatin, S. Mochalov, G. Pugachev, and L. Rosomakho, "Shock compressibility of dry and water-saturated sand," *Soviet Technical Physics Letters,* vol. 2, pp. 207-208, 1976.
15. E. S. Hertel and G. I. Kerley, "CTH reference manual: the equation of state package," Sandia National Laboratories SAND98-0947, 1998.
16. D. Grady, "P-Alpha Compaction of Sand," *Applied Research Associates, Southwest Division,* 2007.
17. J. W. Swegle and D. E. Grady, "Shock viscosity and the prediction of shock wave rise times," *Journal of Applied Physics*, vol. 58, pp. 692-701, 1985.
18. M. U. Anderson, G. T. Holman, and R. A. Graham "Time-resolved shock compression of porous rutile: wave dispersion in porous solids " *In: High-Pressure Science and Technology. American Institute of Physics, New York*, pp. 1111-1114, 1994.

## DISTRIBUTION

AFRL/MNMW
Attn: Mark L. Green
Tom Brantley
Brad Martin
101 W. Eglin
Suite 135
Eglin AFB, FL 32542-6810

DTRA
Attn: Mike Giltrud (CXS)
Robert Hastie (CXSH)
Seung Lee (CXSH)
8725 John J. Kingman Rd.
Ft. Belvoir, VA 22060-6201

Waterways Experiment Station
Geomechanics and Explosion Effects
Attn: Mark Adley
Rebecca P. Berger
J. Donald Cargile
Stephen Akers
3909 Halls Ferry Road
Vicksburg, MS 39180-6199

| | | | |
|---|---|---|---|
| 1 | MS0325 | D. A. Hoke | 2627 |
| 1 | MS0372 | J. E. Bishop | 1525 |
| 1 | MS0751 | L. S. Costin | 6315 |
| 1 | MS1160 | D. A. Dederman | 5431 |
| 1 | MS1160 | A. Fortier | 5431 |
| 1 | MS1160 | J. T. Foster | 5431 |
| 1 | MS1160 | E. W. Klamerus | 5431 |
| 1 | MS1160 | J. E. Lucero | 5431 |
| 1 | MS1160 | V. K. Luk | 5431 |
| 1 | MS1160 | J. S. Ludwigsen | 5431 |
| 1 | MS1161 | D. C. Craft | 5432 |
| 1 | MS1164 | P. C. Butler | 5400 |
| 1 | MS1181 | J. L. Brown | 1646 |
| 1 | MS1181 | C. A. Hall | 1646 |
| 1 | MS1181 | L. C. Chhabildas | 1647 |
| 1 | MS1181 | T. J. Vogler | 1647 |

| | | | |
|---|---|---|---|
| 1 | MS1181 | W. D. Reinhart | 1647 |
| 1 | MS1181 | T. F. Thornhill | 1647 |
| 1 | MS1181 | S. C. Alexander | 1647 |
| 1 | MS1185 | G.C. Bessette | 5417 |
| 1 | MS1322 | S. Silling | 1435 |
| | | | |
| 2 | MS9018 | Central Technical Files | 8944 |
| 2 | MS0899 | Technical Library | 9536 |